

Is the interdecadal variation of the summer rainfall over eastern China associated with SST?

Dong Si^{1,2} · Zeng-Zhen Hu³ · Arun Kumar³ · Bhaskar Jha^{3,4} · Peitao Peng³ · Wanqiu Wang³ · Rongqing Han¹

Received: 4 November 2014 / Accepted: 16 March 2015 / Published online: 26 March 2015
© Springer-Verlag Berlin Heidelberg 2015

Abstract The present study examined the major features of the interdecadal variation of the summer rainfall over eastern China (IVRC) and the possible association with sea surface temperature (SST). We noted that the first leading mode of IVRC (accounting for nearly half of the total variance and with maximum loading for the summer rainfall anomalies over South China) may be not forced by SST. On the other hand, the second and third leading modes [accounting for 17.1 and 13.6 % of the total variance and mainly associated with the summer rainfall anomalies over the Yangtze River valley (YRV) and North China, respectively] in some extent are forced by SST anomalies. These observational results are confirmed by atmospheric general circulation model (AGCM) simulations forced by observed SST. By eliminating the internal dynamical process driven rainfall though ensemble mean, the simulations further suggest an overall enhancement of the intensity of IVRC in the corresponding ensemble mean, especially in the YRV and North China regions, but not in South China. That implies the different role of SST in driving IVRC over different regions.

Keywords Interdecadal variation · Eastern China · Summer rainfall · SST · AGCM · Atmospheric internal dynamics

1 Introduction

With the increase of the observed record length and rapid development in climate models, the understanding of the interdecadal time scale climate variation has improved considerably, particularly, for the interdecadal variations in the twentieth century. For example, a remarkable interdecadal shift was observed in the late 1970s. Numerous studies revealed that this interdecadal shift may be associated with tropical Pacific sea surface temperature (SST) forcing (Graham et al. 1994). Since the late 1970s, SSTs in the tropical eastern and central Pacific have increased, and the Pacific North America (PNA) teleconnection pattern has strengthened during the same time (Nitta and Yamada 1989). The atmospheric general circulation model (AGCM) forced by observed SST reproduced the interdecadal variation of the atmospheric circulation in the Northern Hemisphere (NH) in the late 1970s (Graham 1994), suggesting the important role of SST in the interdecadal climate variations. It is now well established that the link between the interdecadal variation of the atmospheric circulation in NH and the tropical Pacific SST is primarily the tropical-mid-latitude teleconnection (Trenberth 1990; Trenberth and Hurrell 1994; Graham et al. 1994).

On regional scale, climate over eastern China that is greatly influenced by the NH atmospheric circulation also exhibits remarkable interdecadal characteristics. For example, the temperature and rainfall over eastern China had obvious decadal (10–14 years) and interdecadal (30–40 years) time scale variations (Wang et al. 2005).

✉ Dong Si
sidong@cma.gov.cn

¹ National Climate Center, China Meteorological Administration, No. 46 Zhongguancun South Street, Haidian District, Beijing 100081, China

² Collaborative Innovation Center on Forecast and Evaluation of Meteorological Disasters, Nanjing University of Information Science and Technology, Nanjing, China

³ Climate Prediction Center, NCEP/NOAA, College Park, MD, USA

⁴ INNOVIM, LLC, Greenbelt, MD, USA

Furthermore, the summer rainfall over eastern China experienced a major shift in the late 1970s (Hu 1997), and additional shifts in early 1990s and mid-1960s (Ding et al. 2008; Wu et al. 2010). The notable interdecadal shift in the late 1970s was characterized by summer rainfall increased in the Yangtze River valley (YRV; 28° – 32° N, 100° – 122° E) and decreased in North China (Nitta and Hu 1996; Hu 1997). Nitta and Hu (1996) and Hu (1997) emphasized the contribution of global SST, particularly in the tropical western Pacific and Indian Oceans to this interdecadal variation. Chang et al. (2000) also pointed out that the interdecadal variation of SST in the tropical Pacific Ocean may account for the observed variations in the western Pacific subtropical high and rainfall in YRV in the late 1970s.

Another interdecadal shift over eastern China occurred in 1992/93. Wu et al. (2010) noticed that the summer rainfall mainly over South China experienced a pronounced interdecadal variation around 1992/93: The rainfall was below (above) normal during 1980–1992 (1993–2002). Wu et al. (2010) suggested that this interdecadal variation was only weakly influenced by SST in the equatorial Indian Ocean, but not in the tropical Pacific Ocean. Nevertheless, recently, Si and Ding (2013) argued that SST cooling in the tropical central and eastern Pacific, together with the Tibetan Plateau warming, enhanced the land–ocean thermal contrast and intensified the East Asian summer monsoon, which may be responsible for the interdecadal weakening in the summer rainfall over the YRV in the late 1990s.

Clearly, the connection of IVRC with SST variability is still controversial (Nitta and Hu 1996; Hu 1997; Chang et al. 2000; Ding et al. 2008; Wu et al. 2010; Si and Ding 2013). In this work, by analyzing both the observational data and model simulations, we further examine links between IVRC and SSTs. This work is organized as follows: The AGCM, numerical experiment and datasets used in this study are described in Sect. 2. Section 3 examines the major features of IVRC as well as their association with SST in observations. The simulation of IVRC and its association with SST by the National Centers for Environmental Prediction (NCEP) AGCM is given in Sect. 4. A summary and discussion are provided in Sect. 5.

2 Model, experiment and data description

The model data used in this study is from Atmospheric Model Intercomparison Project (AMIP)-type simulations. The model simulations are from the atmospheric component (Global Forecast System: GFS) of the NCEP Climate Forecast System version 2 (Kumar et al. 2012; Saha et al. 2014). A simplified Arakawa Schubert deep convection and shallow convection with an updated mass flux scheme are included in the sub-grid physical process of GFS. The

AGCM has 64 vertical levels (from the surface to 0.26 hPa) in a hybrid sigma-pressure coordinate and a horizontal resolution at T126 (105-km grid spacing).

The AMIP experiments consisted of an ensemble of 18 runs that start from 18 different atmosphere initial conditions on 1st January 1957. For each run, the same observed evolution of SST, sea ice and observed time-evolving greenhouse gas concentrations were prescribed as external forcings. The AGCM was integrated from 1957 to 2013. The simulated summer (June–July–August) precipitation amounts over eastern China from the individual AGCM members and their ensemble mean are examined in this work.

Observed monthly mean rainfall data from 1957 to 2013, provided by China Meteorological Administration (CMA), included information from 160 stations, of which we chose 138 stations located in eastern China (east of 100° E). Geographical location of the 160 stations over China is relatively homogeneously distributed, especially in eastern China (see Hu et al. 2003; Fig. 1a). In addition, the observed monthly mean SST data is used to examine the possible association of IVRC with global SST. The SST fields are derived from National Oceanic and Atmospheric Administration/National Climatic Data Center Extended Reconstructed SST (ERSST) dataset (Smith and Reynolds 2004) for the period of 1957–2013.

To isolate the interdecadal variation, a 15-year low-pass filter was applied to the observed and model simulated rainfall data (Mann et al. 1995). The low-pass filtered rainfall data is used to compare with variance of total rainfall data and for empirical orthogonal function (EOF) analysis.

3 IVRC in the observations

3.1 Variance and leading modes of IVRC

Before we discuss the interdecadal variation of the summer rainfall over eastern China (IVRC), we present some diagnostics of the interdecadal component in the IVRC and their relative strength in the summer rainfall over eastern China. Figure 1a shows the total variance of summer (June, July, August: JJA) rainfall over eastern China derived from the observed station data. The maximum summer rainfall variances are located over the South China (20° – 26° N, 106° – 120° E), YRV and Huai River valley (32° – 35° N, 110° – 122° E), whereas the variance in North China (35° – 40° N, 110° – 120° E) and northeastern China (40° – 50° N, 120° – 130° E) are relative small. Figure 1b is the corresponding variance for the interdecadal component. The maximum interdecadal rainfall variance resides in South China and middle and lower reaches of YRV.

To quantify the relative strength of the interdecadal time scale variations, the ratios of the interdecadal component

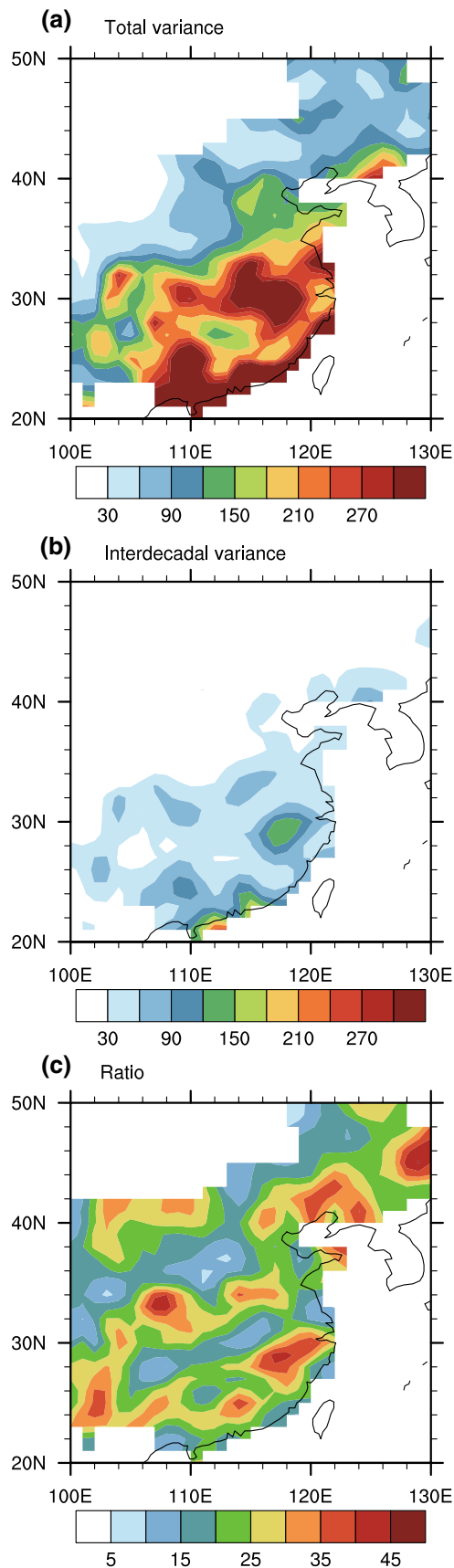


Fig. 1 Variance of total (a) and interdecadal component (b) of the summer (JJA) rainfall over eastern China derived from the observed data and the ratio of the interdecadal component variance to the total variance of the summer rainfall over eastern China (c). The unit is mm^2 in (a, b) and % in (c)

variance to the total variance are shown in Fig. 1c. The ratio exceeding 25 % are located over South China, middle and lower reaches of the YRV, Huai River valley, North China, Northeast China and Inner Mongolia, suggesting the importance of interdecadal component over these regions.

To reveal spatial pattern and the temporal variation of IVRC, the EOF analysis was applied to the 15-year low-pass filtered summer rainfall anomalies. The three leading EOF modes and their corresponding principal components (PCs) are shown in Fig. 2. They account for 44.6, 17.1 and 13.6 % of the total variance, respectively. The accumulated variance of the first three modes accounts for 75.3 % of total interdecadal variance, implying that the first three modes represent the major part of IVRC.

For the first EOF mode (EOF1), it is dominated by variation over South China, whereas opposite variation is seen over northern China (north of 30°N). The corresponding PC (PC1) exhibits remarkable interdecadal variability: positive from early 1960s to 1970s and early 1990s to early 2000s, and negative from 1980s to early 1990s and mid-2000s to early 2010s. The interdecadal shift around early 1990s shown in PC1 is consistent with Wu et al. (2010). They noticed the summer rainfall over South China changed from below normal to above normal around 1992/93.

EOF2 mainly reflects the interdecadal variation in YRV. There are two remarkable abrupt phase transitions in PC2. One is around late 1970s (from negative to positive) and the other is around late 1990s (from positive to negative). The former abrupt phase transition coincides temporally with the significant interdecadal shift in the global atmospheric-oceanic system (Graham 1994; Kachi and Nitta 1997; Hu 1997) as well as in East Asia (e.g. Nitta and Hu 1996; Hu 1997; Chang et al. 2000; Gong and Ho 2002; Ding et al. 2008). The latter phase transition indicates the summer rainfall has decreased over the YRV but increased over the Huai River valley and South China since the late 1990s, consistent with Si et al. (2009) and Si and Ding (2013). Compared with PC1, PC2 has higher frequency. Importantly, the amplitude of PC2 increases with time, which may imply an intensifying trend in interdecadal variation component of summer rainfall over YRV.

EOF3 has small spatial loading and small fraction (13.6 %) of total variance explained. Some positive loadings are located over the YRV, and negative ones over other parts of eastern China.

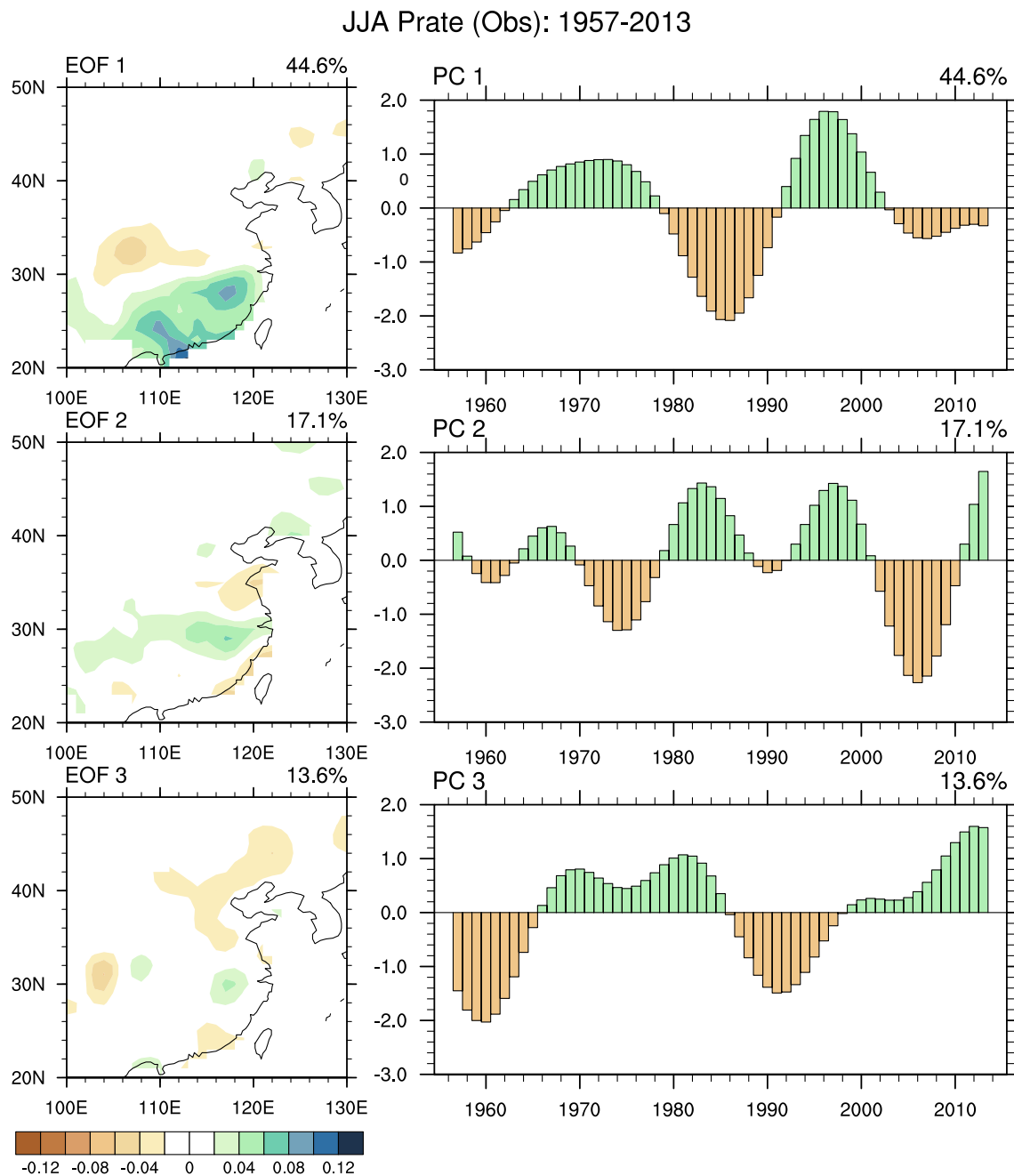


Fig. 2 Spatial pattern of the three leading EOF modes for a 15-year low-pass filtered observed summer (JJA) rainfall over eastern China and their corresponding time coefficients during 1957–2013

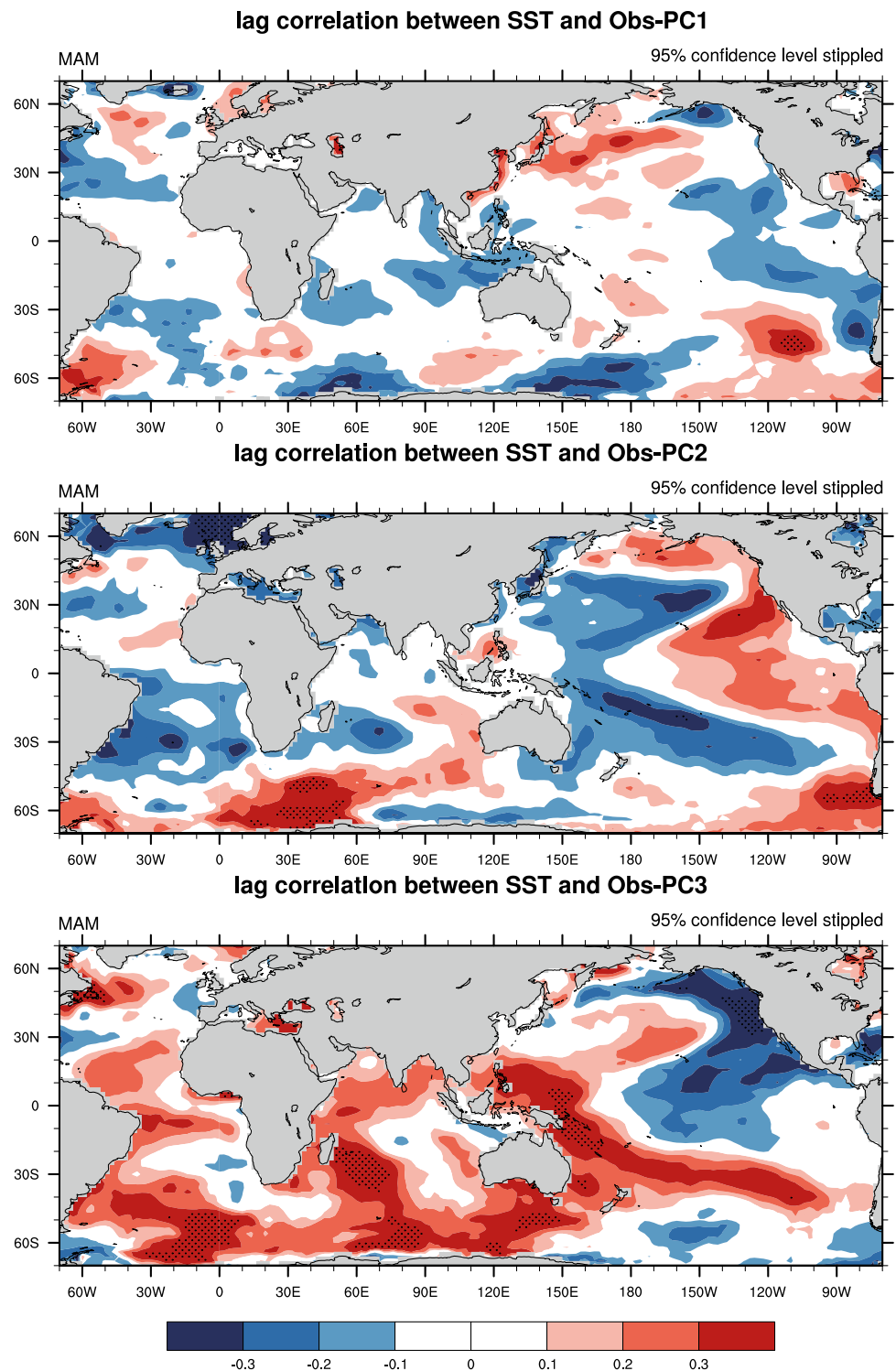
3.2 IVRC-SST relationship

In this section, we examine the possible relationship between the three leading modes of IVRC and SST in the observations. Figure 3 shows the correlations between three PCs for summer rainfall and global SST anomalies in spring (March, April, May: MAM). For PC1, the correlation seems associated with a negative phase of Pacific Decadal Oscillation (PDO)-like pattern in the Pacific Ocean, but all correlations

are not significant. That suggests that EOF1 of IVRC may be not forced by the interdecadal variation of SST anomalies, instead it may be driven by the atmospheric internal dynamics. This hypothesis will be further verified and confirmed by the analysis of model simulations discussed in Sect. 4.2.

For PC2, the correlations are a seesaw-like pattern in Southern Hemisphere (SH) with positive correlation over the south-polar region and negative one over the mid-latitude in SH. That may suggest a possible connection of the evolution

Fig. 3 Correlations between the time coefficients of the three leading EOF modes for a 15-year low-pass filtered observed summer (JJA) rainfall over eastern China (Fig. 2) and the observed global SST anomalies in spring (MAM) during 1957–2013



of this mode with variability in the south-polar region, such as the Antarctic Oscillation (AAO). In fact, Nan and Li (2003) had pointed out a positive correlation between AAO index and summer rainfall anomaly in YRV. Statistically, positive phase of AAO is followed by a weakened East Asian summer monsoon, a westward and strengthened expanded northwestern Pacific subtropical high, as well as increased

water vapor convergence and ascending vertical velocity. These anomalies provide large-scale atmospheric circulation and vapor condition favorable to above-normal summer rainfall over YRV, and vice versa. It is argued that AAO might serve as an atmospheric bridge that link interdecadal variation of summer rainfall in YRV (EOF2 of IVRC) and the seesaw-like SST anomalies in SH. In addition, the

correlation also shows an El Niño-like pattern in the tropical Pacific Ocean, although the correlation is weaker than that in SH. That implies that EOF2 of IVRC may also be associated with the interdecadal variation of ENSO in some extent.

As for PC3, there are positive correlations in the Indo-Pacific and South Atlantic Oceans, suggesting that the SST in these regions might influence the evolution of EOF3 of IVRC. The correlations between 1000 hPa geopotential height field and interdecadal scale filtered SST index of Indo-Pacific and South Atlantic Oceans (0° – 70° S, 60° W– 180° E) (Figure not shown) suggest that in response to warming in the Indo-Pacific and South Atlantic Oceans,

the geopotential height increases and an anomalous anti-cyclonic circulation forms over northern China, collocated and consistent with the negative rainfall anomalies in the region (bottom panel in the left, Fig. 2).

4 Simulations of IVRC

4.1 Leading modes of IVRC

To investigate to what extent IVRC is influenced by SST forcing, we use the AGCM simulations forced by the

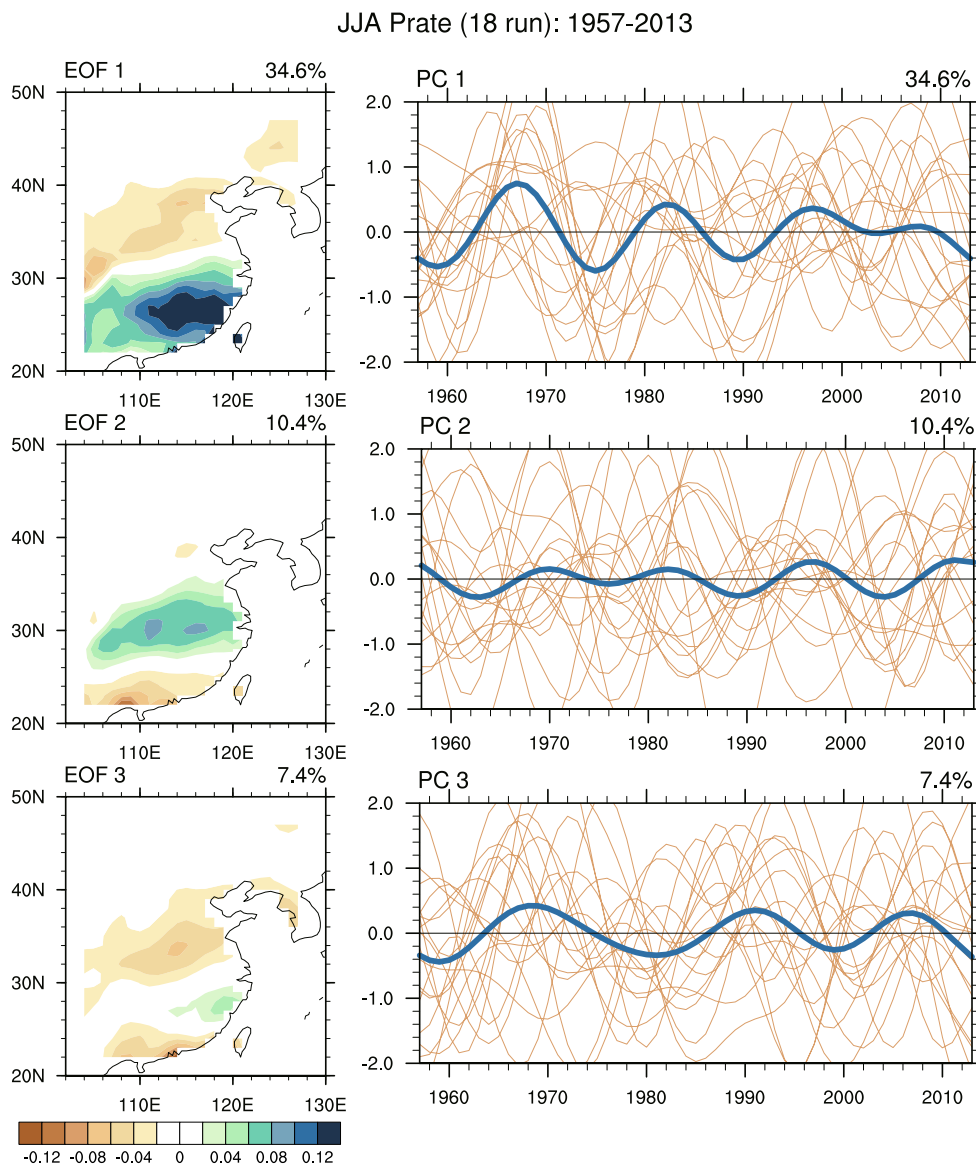


Fig. 4 Spatial pattern of the three leading EOF modes for a 15-year low-pass filtered summer (JJA) rainfall over eastern China simulated by the NCEP AGCM and their corresponding time coefficients during 1957–2013. The thin dash curves represent the 18 members' corre-

sponding time coefficients and the thick solid curve is the ensemble mean of the 18 member's corresponding time coefficients for each EOF mode

Table 1 Spatial correlation coefficients between the three leading EOF modes (EOF1, EOF2 and EOF3) for a 15-year low-pass filtered summer (JJA) rainfall over eastern China that simulated by the NCEP AGCM (Fig. 4) and that derived from the observed data (Fig. 2)

	EOF1-Obs	EOF2-Obs	EOF3-Obs
EOF1-AGCM	0.77*	0.11	0.41*
EOF2-AGCM	-0.32*	0.61*	0.22
EOF3-AGCM	0.23	0.17	0.27

The values with “*” are significant at a significance level of 99 %

observed global SST to complement results based on the observations. In order to extract the leading modes of IVRC simulated by the model, the time-series from 18

individual ensemble members’ is concatenated into a single time-series, then a conventional EOF analysis is applied to the concatenated array. The derived PC for each EOF mode will contain 18 consecutive sequential time evolution representing temporal evolution of each mode simulated by 18 individual simulations. PCs for each simulation are shown in Fig. 4 as the thin dash curve, and the thick solid curve is the average of the 18 member’s PCs.

Figure 4 shows the three leading EOF modes of IVRC and the corresponding PCs simulated by the model. For EOF1, the model reproduces the spatial pattern of the observed EOF1 (Fig. 2), which is dominated by the anomalies in South China and characterized by some opposite variations in 30–40°N. The spatial correlation of EOF1

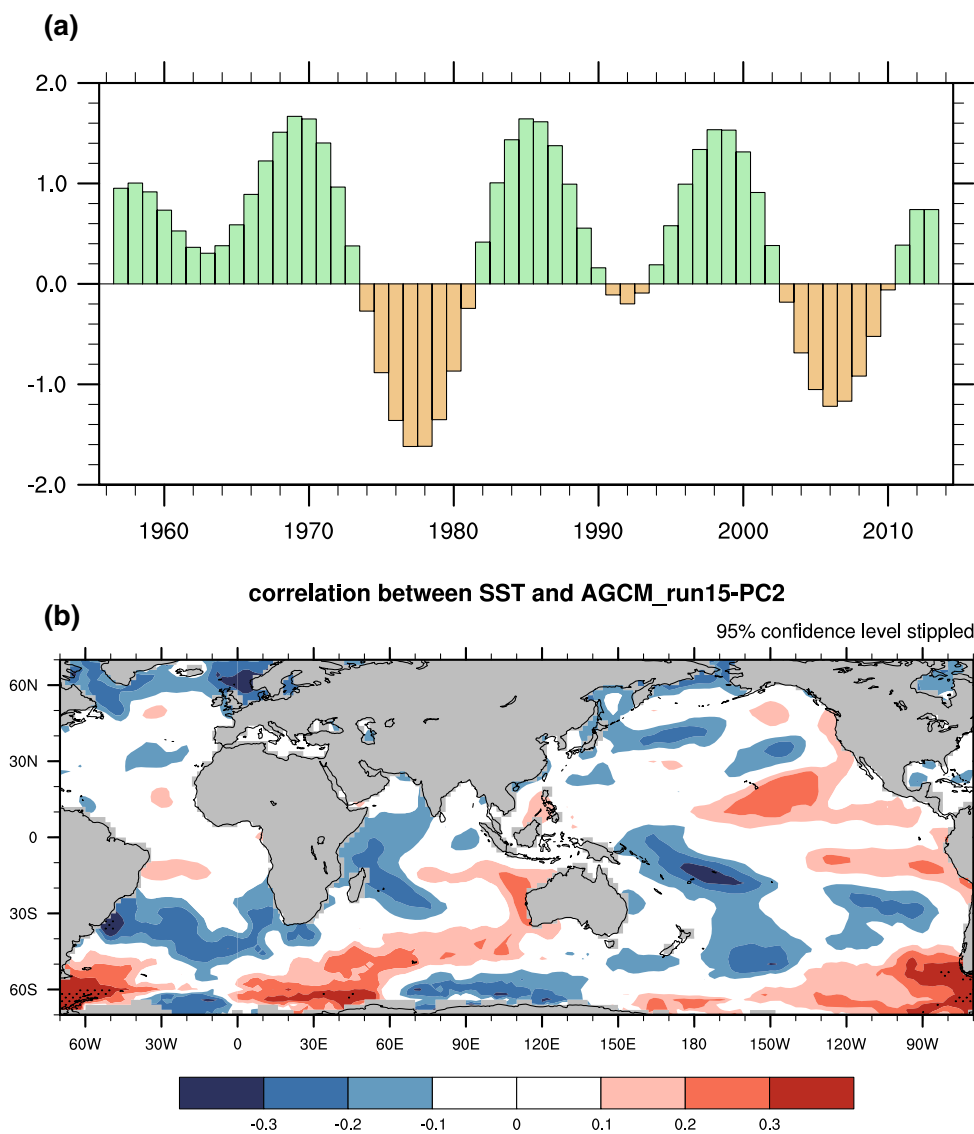


Fig. 5 The corresponding time coefficient of the second EOF mode for a 15-year low-pass filtered summer (JJA) rainfall over eastern China simulated by the member-15 of the NCEP AGCM (a) and its correlations with the observed global SST in spring (MAM) during 1957–2013 (b)

between the simulation and observation is 0.77 (Table 1). However, although the pattern of EOF1 is well simulated by the model, its temporal evolution is not well captured either by individual members or by the ensemble mean. About the reason that the model reproduced the spatial pattern of EOF1 but not the evolution (PC1), we speculate that may be the result of a common default of state-of-the-art of climate models. For example, Jha et al. (2014) noted that most of ten coupled models in Coupled Model Intercomparison Project Phase 5 (CMIP5) they analyzed well simulated the spatial variation pattern of SST associated with ENSO, but almost no one captured the spectrum of ENSO.

For EOF2, the model also captured the spatial pattern with pattern correlation of 0.61 between the simulation and observation (Table 1). The temporal correlation of PC2 between the ensemble mean and the observation is 0.41, may suggest some impact of SST anomalies on the evolution of EOF2. Interestingly, among the 18 members, some of them (for example member-15) well captured the time evolution of EOF2 (PC2) and its association with global SST anomalies (Fig. 5). For example, the correlation of PC2 between the observation and ensemble member-15 reaches 0.68. A moderate correlation with the ensemble mean and high correlation with one specific ensemble member (member 15) may imply that the SST and atmospheric initial condition as well as atmospheric internal dynamics all play a role in the evolution of EOF2.

For EOF3, the model produces the corresponding spatial pattern in the observations to some extent with pattern correlation 0.27 between the observations and the simulations. However, the temporal evolution of the mode (PC3) is not captured.

Additionally, in order to confirm this result, we project the model ensemble mean rainfall onto EOFs 1-3 of the observations. By this way, we can further examine if the EOF modes are reproduced by the model. Figure 6 shows the time series of the projection. Compared the time series with the PCs 1-3 in the observations (right panel, Fig. 2), we can find that the temporal evolution of the time series of the projection does not match the PCs 1-3 in the observation well. The correlations between the PCs 1-3 in the observation and the corresponding time series of the projection are 0.16, 0.34 and 0.5, respectively. The correlations also consist with the associations of the corresponding modes with SST anomalies in the observations discussed in Sect. 3.2. Moreover, the weak correlations are consistent with large spread of PC1-3 among the individual ensemble members (right panels of Fig. 4), implying that the overall influence of SST on the temporal evolutions of these IVRC modes are small and the atmospheric internal dynamics may play a more important role.

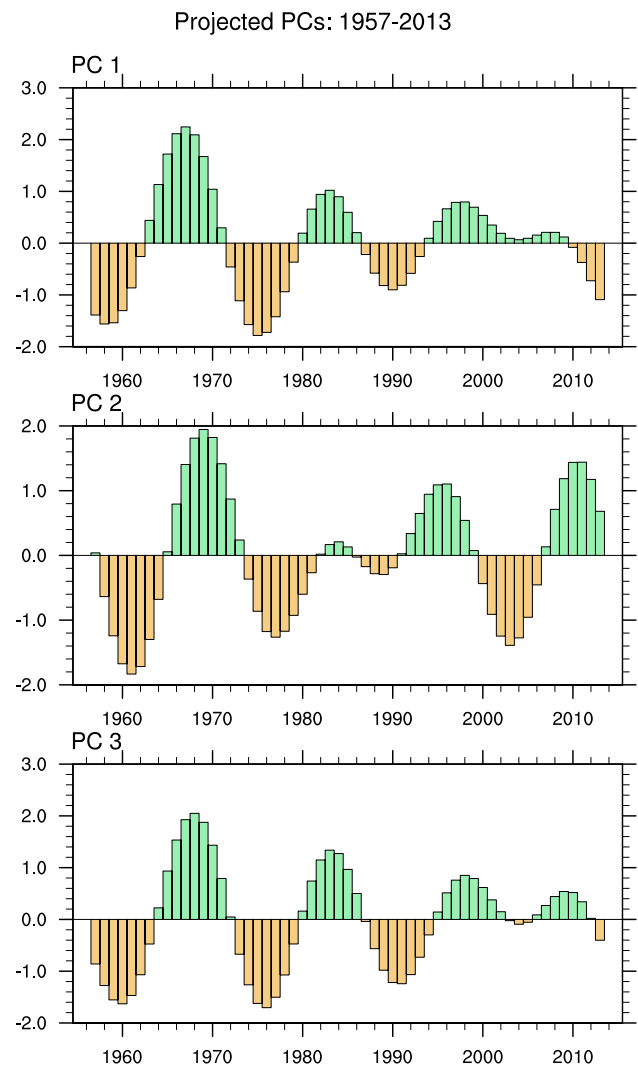


Fig. 6 Time series of the projection of the NCEP AGCM model ensemble mean summer (JJA) rainfall onto the three leading EOF modes in the observation

4.2 Simulation of IVRC-SST relationship

The above results suggest that the evolution of EOF1 may not be forced by SST, while the EOF2 and EOF3 of IVRC may be associated with SST. To further elaborate this result, a correlation analysis was also conducted to the global SST and PCs 1-3 of the model ensemble mean. Similar to the observations (top panel, Fig. 3), all correlations of SST anomalies with PC1 of model ensemble mean are not significant at 95 % confidence level (top panel, Fig. 7), confirming that the evolution of EOF1 (mainly the interdecadal variation of summer rainfall over South China) is not forced by SST and may be driven by atmospheric internal dynamics.

For EOF2 (middle panel, Fig. 7), the model can't reproduce the correlation pattern and amplitude in the

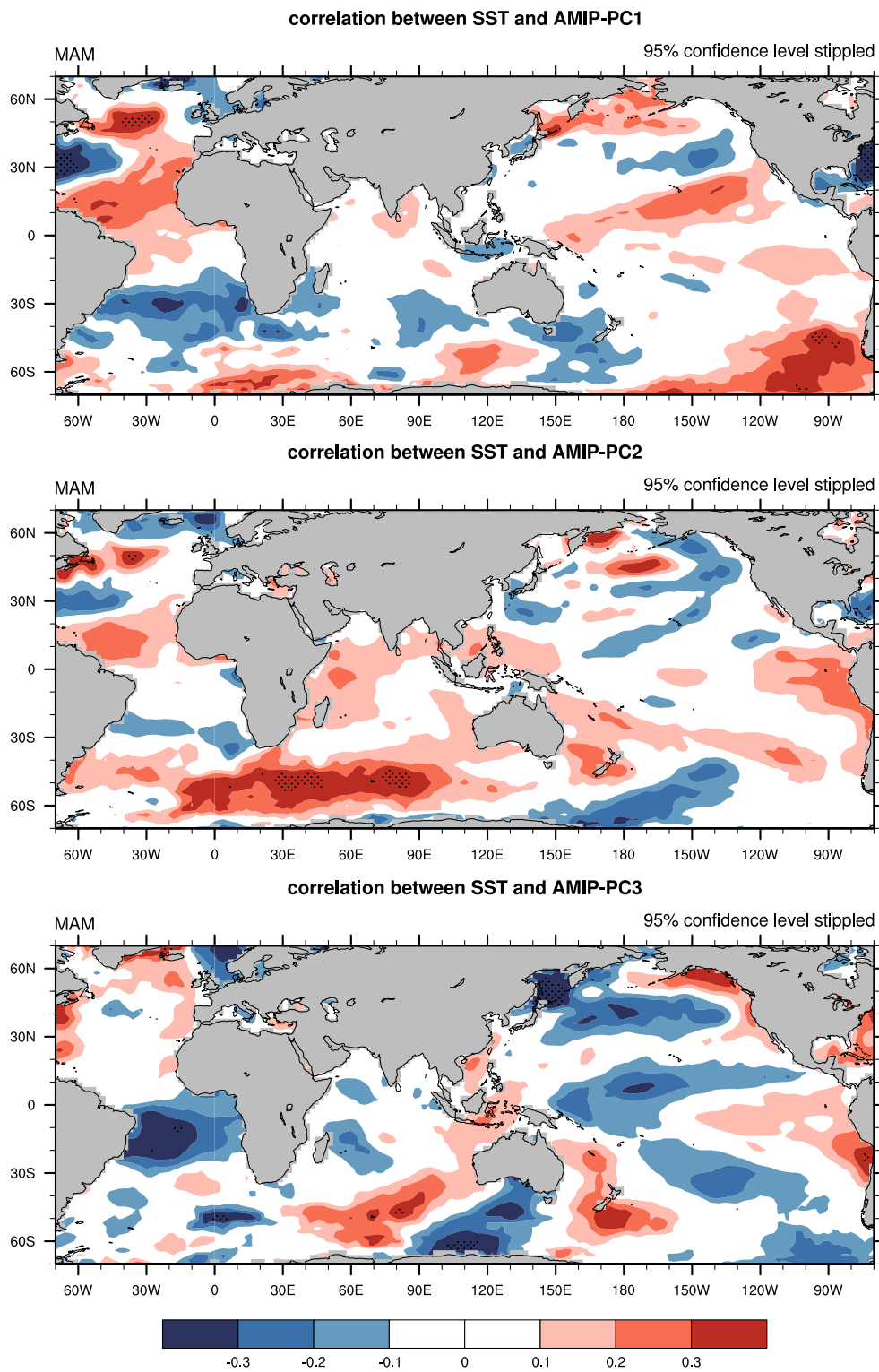


Fig. 7 Correlation between the ensemble mean time coefficients of three leading EOF modes for a 15-year low-pass filtered summer (JJA) rainfall over eastern China simulated by the 18 members of

the NCEP AGCM and the observed global SST anomalies in spring (MAM) during 1957–2013

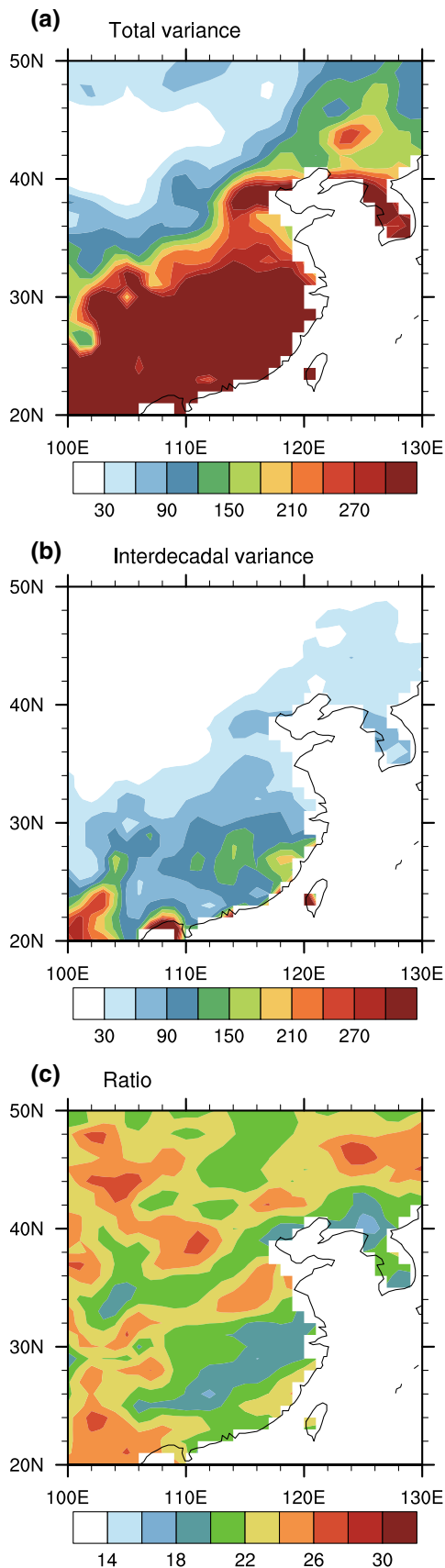


Fig. 8 Mean variance of total (a) and interdecadal component (b) of the summer (JJA) rainfall over eastern China for 18 individual members of the NCEP AGCM and the ratio of the interdecadal component variance to the total variance of the summer rainfall over eastern China (c). The unit is mm^2 in (a, b) and % in (c)

observations (middle panel, Fig. 3), particularly the see-saw-like SST anomaly pattern in SH. Similarly, the model also didn't simulate the connection between PC3 and SST in the Indo-Pacific and South Atlantic Oceans in the observations. The failure of the model in simulating the connection between EOF2/EOF3 and SST anomalies may be partially due to model biases. Also it is possible that the connections seen in the observations are not robust and is an artifact of small sample (i.e., short data length). On the other hand, the good reproduction of the temporal evolution of EOF2 and its association with SST anomalies by ensemble member 15 (Fig. 5) seems to suggest that both SST anomalies and atmospheric initial condition may play some role.

4.3 SST enhancement to IVRC

In this subsection, we further examine the impact of SST on IVRC by comparing the variance of summer rainfall over eastern China in individual ensemble members and in ensemble mean. Figure 8 shows the average of variance of 18 individual ensemble members for total and interdecadal component and their ratios. While Fig. 9 is the corresponding ones for the variability of the ensemble mean. For both the total and interdecadal component variance and their ratios, the model's individual ensemble member (Fig. 8) reproduces both the spatial pattern and amplitude in the observations (Fig. 1), suggesting the reliability of the model simulations.

Nevertheless, the amplitudes of variance for both the total and interdecadal component decrease significantly for the ensemble mean (compared top and middle panels of Fig. 9 with Figs. 1, 8), due to the fact that the atmospheric internal dynamical processes that unrelated to SST forcing driven rainfall are largely eliminated by the ensemble mean. Furthermore, the overall amplitude of the ratio of the interdecadal component variance to the total variance increases for the ensemble mean compared with the individual member (Figs. 8c, 9c). Specifically, the ratio increases remarkably in YRV and North China and doesn't change much in South China (compared Fig. 9c with 8c). This suggests that by eliminating the atmospheric internal dynamical processes that unrelated to the SST forcing, the fraction of interdecadal variation increases in YRV and North China and doesn't change much in South China, implying that

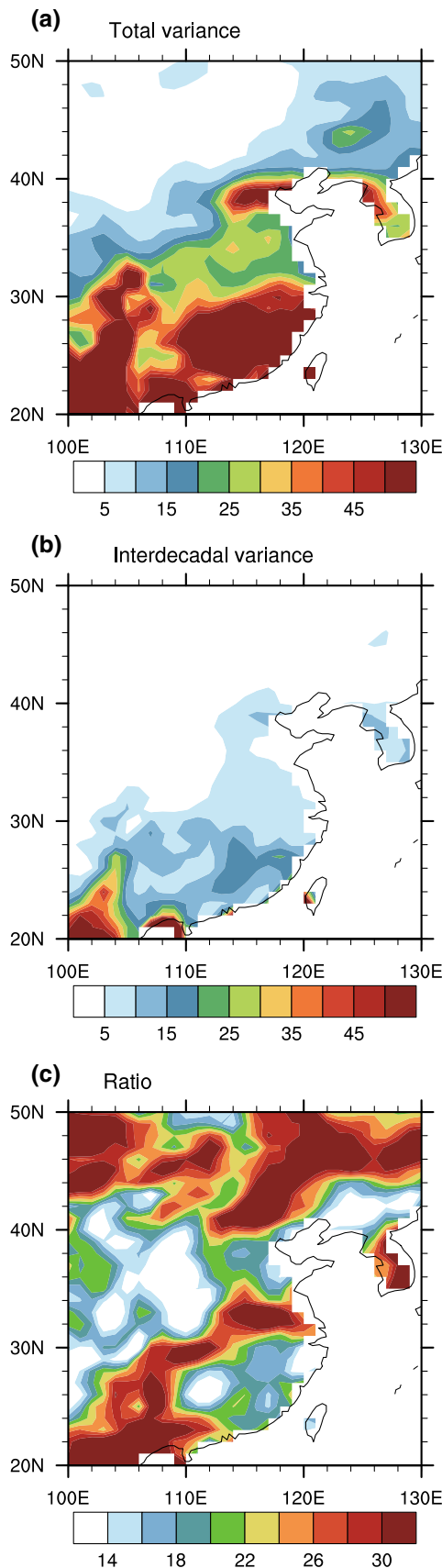


Fig. 9 Variance of total (a) and interdecadal component (b) of the summer (JJA) rainfall over eastern China for the 18 member ensemble mean and the ratio of the interdecadal component variance to the total variance of the summer rainfall over eastern China (c). The unit is mm² in (a, b) and % in (c)

the interdecadal variation of summer rainfall in YRV and North China is forced by SST, but the interdecadal variation in South China is not associated with SST and may be driven by the atmospheric internal dynamics. This is generally consistent with the above results shown in Sect. 3.

5 Summary and discussions

In this study, we examined the major features of IVRC and their association with global SST by analyzing the observational data as well as 18 member AGCM simulations runs forced by the observed SST. The EOF analysis suggests that EOF1 of IVRC is dominated by summer rainfall anomalies in South China, which is largely driven by atmospheric internal dynamical processes and not by SST anomaly. EOF2 of IVRC mainly represents summer rainfall anomalies in YRV and its temporal evolution seems influenced by SST anomaly. Importantly, the amplitude of PC2 shows an increasing trend, suggesting that the intensified trend of interdecadal variation of summer rainfall in YRV. As for EOF3, it accounts for the summer rainfall anomalies in North China and might be also affected by SST.

The AGCM runs capture all the spatial patterns of the observed three leading EOF modes, but not their temporal evolutions. Analysis of the model runs confirms the independence of EOF1 to SST forcing, suggesting that the interdecadal variation of summer rainfall in South China is largely atmospheric internal dynamics driven. Furthermore, model results also suggest that the fraction of interdecadal component increased in YRV and North China, but not in South China with SST forcing, suggesting that the impact of SST on the interdecadal variations of summer rainfall may depend on regions. That may also imply that the interdecadal variations of summer rainfall in different regions may be associated with different physical processes. In addition, the fact that some ensemble member can capture the time evolution of the observed EOF2 of IVRC seems to suggest that the SST and atmospheric initial condition as well as atmospheric internal dynamics all play a role in the interdecadal variation of summer rainfall over YRV. It should be pointed out that the correlations we discussed here are simultaneous or one season lag correlations. For the longer delayed possible impact of SST on IVRC, it is a future research topic. Also, short lengthen of the data for

examining the interdecadal variations may affect robustness of the EOF patterns analyzed in this work, particularly for the higher order mode (EOF 2 and 3). For the model simulations, it is still a challenge to capture some regional climate features. And the impact of model bias on the climate in East Asia is another open question (Kumar et al. 2012).

In fact, in addition to the impact of model biases, without fully air-sea coupling (or the feedback from the atmosphere to the ocean) in the AMIP runs may also affect the results shown in this work in some extent. For example, Wang et al. (2005) showed that a free run of a coupled ocean–atmosphere general circulation model (CGCM) realistically simulated rainfall–SST relationship in the Asian-Pacific monsoon region. However, when the AGCM forced by the prescribed same SST, it fails to reproduce the relationship, suggesting that coupled ocean–atmosphere process is crucial in the simulation of rainfall interannual variability in Asian-Pacific monsoon region. Zhu and Shukla (2013) further indicated that lacking of ocean–atmosphere coupling process is a major source of biases resulting in an unrealistic rainfall–SST relationship over the Asian-Pacific monsoon region at interannual time scales. These works demonstrated the necessity of using an ocean–atmosphere coupled prediction system in order to predict or simulate the interannual variability of summer rainfall over the Asian-Pacific monsoon region. Nevertheless, it is unclear how important of air-sea coupling in the interdecadal variation of summer rainfall in eastern China.

Acknowledgments Most of this work was finished during a visit to the Climate Prediction Center, NCEP/NOAA. This research is jointly supported by the National Basic Research Program of China (2013CB430202, 2012CB955203), the National Natural Science Foundation of China (41405071) and the CMA Special Public Welfare Research Fund (GYHY201406001). Thanks also go to two anonymous reviewers for their constructive suggestions.

References

- Chang CP, Zhang Y, Li T (2000) Interannual and interdecadal variations of the East Asian summer monsoon and tropical Pacific SSTs. Part I: role of subtropic ridges. *J Clim* 13:4310–4325
- Ding Y, Wang Z, Sun Y (2008) Inter-decadal variation of the summer rainfall in East China and its association with decreasing Asian summer monsoon. Part I: observed evidences. *Int J Climatol* 28:1139–1161
- Gong DY, Ho CH (2002) Shift in the summer rainfall over the Yangtze River valley in the late 1970s. *Geophys Res Lett* 29:1436. doi:10.1029/2001GL014523
- Graham NE (1994) Decadal-scale climate variability in the tropical and North Pacific during the 1970s and 1980s: observations and model results. *Clim Dyn* 10(3):135–162
- Graham NE, Barnett TP, Wilde R et al (1994) On the roles of tropical and mid-latitude SSTs in forcing interannual to interdecadal variability in the winter Northern Hemisphere circulation. *J Clim* 7:1416–1441
- Hu Z-Z (1997) Interdecadal variability of summer climate over East Asia and its association with 500 hPa height and global sea surface temperature. *J Geophys Res* 102:19403–19412
- Hu Z-Z, Yang S, Wu R (2003) Long-term climate variations in China and global warming signals. *J Geophys Res* 108:4614. doi:10.1029/2003JD003651
- Jha B, Hu Z-Zhu, Kumar A (2014) SST and ENSO variability and change simulated in historical experiments of CMIP5 models. *Clim Dyn* 42(7–8):2113–2124. doi:10.1007/s00382-013-1803-z
- Kachi M, Nitta T (1997) Decadal variations of the global atmosphere-ocean system. *J Meteorol Soc Jpn* 75:657–675
- Kumar A, Chen M, Zhang L, Wang W, Xue Y, Wen C, Marx L, Huang B (2012) An analysis of the non-stationarity in the bias of sea surface temperature forecasts for the NCEP climate forecast system (CFS) version 2. *Mon Weather Rev* 140:3003–3016
- Mann ME, Park J, Bradley RS (1995) Global interdecadal and century-scale climate oscillations during the past five centuries. *Nature* 378:266–270
- Nan S, Li J (2003) The relationship between the summer rainfall in the Yangtze River valley and the boreal spring Southern Hemisphere annular mode. *Geophys Res Lett* 30:2266. doi:10.1029/2003GL018381
- Nitta T, Hu Z-Z (1996) Summer climate variability in China and its association with 500 hPa height and tropical convection. *J Meteorol Soc Jpn* 74:425–445
- Nitta T, Yamada S (1989) Recent warming of tropical sea surface temperature and its relationship to the Northern Hemisphere circulation. *J Meteorol Soc Jpn* 67:375–383
- Saha S et al (2014) The NCEP climate forecast system version 2. *J Clim* 27:2185–2208. doi:10.1175/JCLI-D-12-00823.1
- Si D, Ding Y (2013) Decadal change in the correlation pattern between the Tibetan Plateau Winter Snow and the East Asian summer rainfall during 1979–2011. *J Clim* 26:7622–7634
- Si D, Ding Y, Liu Y (2009) Decadal northward shift of the Meiyu belt and the possible cause. *Chin Sci Bull* 54:4742–4748
- Smith TM, Reynolds RW (2004) Improved extended reconstruction of SST (1854–1997). *J Clim* 17:2466–2477
- Trenberth KE (1990) Recent observed interdecadal climate change in the northern hemisphere. *Bull Am Meteorol Soc* 71:988–993
- Trenberth KE, Hurrell JW (1994) Interdecadal atmosphere-ocean variations in the Pacific. *Clim Dyn* 9:303–319
- Wang B, Ding Q, Fu X, Kang I-S, Jin K, Shukla J, Doblas-Reyes F (2005) Fundamental challenge in simulation and prediction of summer monsoon rainfall. *Geophys Res Lett* 32:L15711. doi:10.1029/2005GL022734
- Wu R, Wen Z, Yang S, Li Y (2010) An interdecadal change in Southern China Summer Rainfall around 1992/93. *J Clim* 23:2389–2403
- Zhu J, Shukla J (2013) The role of air-sea coupling in seasonal prediction of Asia-Pacific summer monsoon rainfall. *J Clim* 26:5689–5697